Received 17 July 2023; revised 6 September 2023; accepted 10 September 2023. Date of publication 18 September 2023; date of current version 17 October 2023.

Digital Object Identifier 10.1109/OJAP.2023.3316704

A Quad-Polarization and Beam Agile Array Antenna Using Rat-Race Coupler and Switched-Line Phase Shifter

MAODUDUL HASAN (Member, IEEE), EISUKE NISHIYAMA (Member, IEEE), AND ICHIHIKO TOYODA (Member, IEEE)

Faculty of Science and Engineering, Saga University, Saga 840-8502, Japan

CORRESPONDING AUTHOR: MAODUDUL HASAN (e-mail: hasan@ceng.ec.saga-u.ac.jp)

This work was supported in part by JSPS KAKENHI under Grant JP23K03840.

ABSTRACT This paper proposes a quad-polarized microstrip array antenna with beam steering capability. The proposed antenna consists of two patch elements, one rat-race coupler, and two 90° switchable phase shifters. With the aid of just four PIN diodes, the two 90° phase shifters can provide four different diode arrangements for each port of the rat-race coupler. The array elements are excited by using orthogonal feed lines. Due to the combination of the rat-race coupler and phase shifters, different phase conditions are generated between the patch elements or orthogonal modes of the patches. As a result, the proposed antenna can achieve two beams for each of four polarizations, i.e., two circular polarizations (CP) and two linear polarizations (LP). In the case of CP, the antenna can switch the beams between sum and difference radiation patterns. On the other hand, the beam can be tilted to ±15° and ±12° for horizontal and vertical LP states, respectively. A prototype of the antenna is manufactured and measured demonstrating results in accordance with simulation expectations. Measured results indicate that the 10-dB impedance covers from 5.6 to 5.9 GHz and the measured gains range from 7 to 8.5 dBic.

INDEX TERMS Circular and linear polarization, polarization-agile, reconfigurable antenna, switchable feed, pattern reconfigurable, beam-steering antennas.

I. INTRODUCTION

THE COMPACT and multifunctional antenna plays a crucial role as a fundamental element of the rapidly developing fifth-generation (5G) wireless system. Polarization and beam agile antennas are two advanced technologies that can enhance the performance of communication systems. Polarization-agile antennas can be used in many applications, such as polarization diversity, synthetic-aperture-radar (SAR) systems, frequency reuse, sensor systems, multiple-input multiple-output (MIMO) systems, etc. [1]. Dual polarized antennas can transmit and receive information by using their two orthogonal polarizations in the same frequency band, increasing the data rate and improving the signal quality. Besides, the polarization switchable antennas can reduce the effects of multipath interference [2]. Beam switchable antennas, on the other hand, are antennas that can switch between multiple directional beams. This allows the antenna to focus its energy in a specific direction, increasing the signal strength and improving the signal-to-noise ratio. Beam switching can also improve the efficiency of the antenna by reducing interference from unwanted signals [3]. Combining both polarization and beam switchable technologies can further enhance the performance of the communication systems, allowing for more efficient and reliable communication in various applications, such as wireless networks and satellite communication [4], [5], [6].

The 5G of mobile communications new radio (NR) base station (BS) and customer premises equipment (CPE) require three properties, i.e., polarization switching, beam switching, and moderately large bandwidths [5], [7]. Although several reconfigurable antennas can be found in the literature with the features of compactness and low cost, it is still challenging to simultaneously achieve low-profile polarization and beam switchable antennas [8]. The main novelty of this

work lies in its features where it combines all the 5G NR's above-mentioned features in a compact, cheap, and simple layout.

The polarization switchable antennas employ electronic switches [6], [7], [8], [9], [10], [11], [12], [13], [14], [15], [16], switchable polarizer [17], mechanical rotation [18], and optical devices [19]. The electronic switches can redirect antenna currents to switch the antenna's polarization with the advantages of agile tuning, low loss, and flexible control. In the case of electronic switching techniques, several techniques such as reconfigurable feeding networks and controllable perturbation segments in the antenna's structure are used. Most of the polarization agile antennas that are found in the literature can switch between two polarizations. Realizing quad-polarization agile antennas still poses challenges in antenna designs [14]. In [12], [13], [14], quad-polarization switchable antennas are realized by a switchable feed network. Antennas that can switch beams [3], [4], [8], [10], [20], [21], [22], [23], [24], [25] can be achieved through various methods, such as modifying the antenna structure, using phased arrays, and utilizing different feeding ports.

Several antennas with polarization and beam-switching functionality have been reported in the literature. A multi-layer substrate dual circularly polarized antenna with beam-switching functionality using switchable feed networks has been reported in [6]. Authors in [8] proposed another polarization switchable antenna using a metasurface and feeding network with two beam switching states for each polarization with the aid of a ring-shaped pixel structure around the metasurface. In [10], a three-linearly polarization switchable antenna with five beams at each polarization has been achieved. The beam switching for each polarization state is realized by placing multiple electronically reconfigurable parasitic elements in close proximity to the polarization switchable antenna. Most of the reported polarization agile with beam-switching functional antennas have complex structures due to the multi-layer substrate, phase shifting element, a large number of switches, and complex feeding network.

The antenna presented in this work is novel in that it provides dual beam-switching functionality for each quad-polarization states using a compact and switchable feed scheme. The novelty of this work lies in its ability to solve the aforementioned issues of polarization and beam switchable antennas. The proposed concept is designed using just a single layer, less number of diodes, and a simple feeding network. Moreover, the feed structure's efficiency is increased since both the switching components and transmission lines can be shared effectively among different polarization states.

The rest of the paper is structured as follows: Section II discusses the design and operating principle of the proposed antenna, as well as the performance of the antenna element and array. Section III focuses on the fabrication and measurement of the prototype, presenting and analyzing both the simulated and measured results. Finally, conclusions are drawn in Section IV.

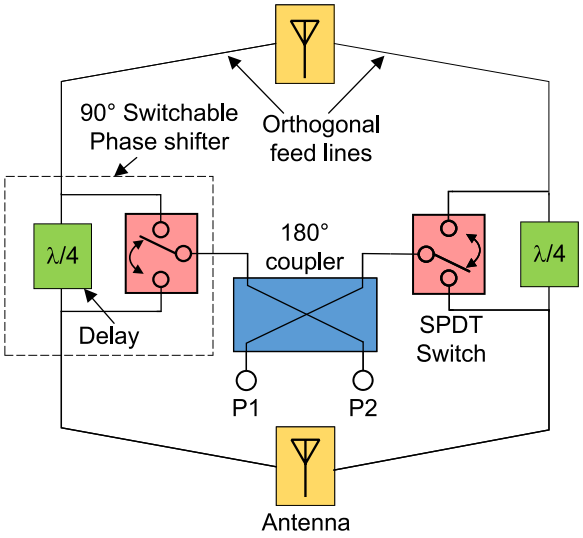

FIGURE 1. Block diagram of the proposed quad-polarization and beam switchable antenna.

II. ANTENNA STRUCTURE AND OPERATIONAL MECHANISM

A. ANTENNA CONFIGURATION

Fig. 1 shows the block diagram of the proposed antenna's concept. The proposed antenna consists of two antenna elements, a 180° hybrid coupler, and two 90° switchable phase shifters. Each 90° phase shifter is realized by a single-pole double-throw (SPDT) switch and quarter-wavelength delay line. Each antenna element is excited by two orthogonal feed lines. The 180° coupler splits input signals equally but in- or anti-phase to its output ports based on its input ports. The 90° phase shifter again divides the signal equally but creates a 90° phase difference between the antenna elements. The antenna elements are excited with equal amplitude but with different phase relationships using the orthogonal feed lines. Due to the different phase difference conditions either between the antenna elements or orthogonal feed lines, the proposed concept can provide multi-functionality in a low profile.

Fig. 2 shows the geometrical configuration and cross-sectional view of the proposed antenna. The antenna is designed following the concept where the rat-race coupler realizes the 180° coupler. The rat-race coupler has two input ports, P1 and P2, and two output ports. The output ports connect with the SPDT switch. The SPDT switch has two $\lambda/2$ branches where two PIN diodes are mounted in opposite directions at the end of each branch. The two branches are connected at $\lambda/4$ distance from each other of the microstrip line that connects to the patch elements #1 and #2. To control the SPDT switches independently, two bias voltages V1 and V2 and capacitors are required. The bias voltage is provided from the bias pad following an inductor. Two vias at

TABLE 1. Operational modes of the proposed antenna.

	Port 1				Port 2			
Operating Modes	I	II	III	IV	V	VI	VII	VIII
ON Diode	D2, D4	D1, D3	D2, D3	D1, D4	D2, D4	D1, D3	D2, D3	D1, D4
Polarization.	RHCP	LHCP	HLP	HLP	LHCP	RHCP	VLP	VLP
Peak Angle ($\phi = 90°$)	Sum	Sum	$+\theta_m$	$-\theta_m$	Difference	Difference	$-\theta_m$	$+\theta_m$
Beam	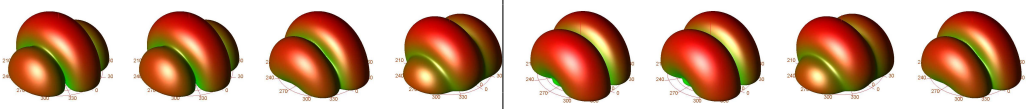							

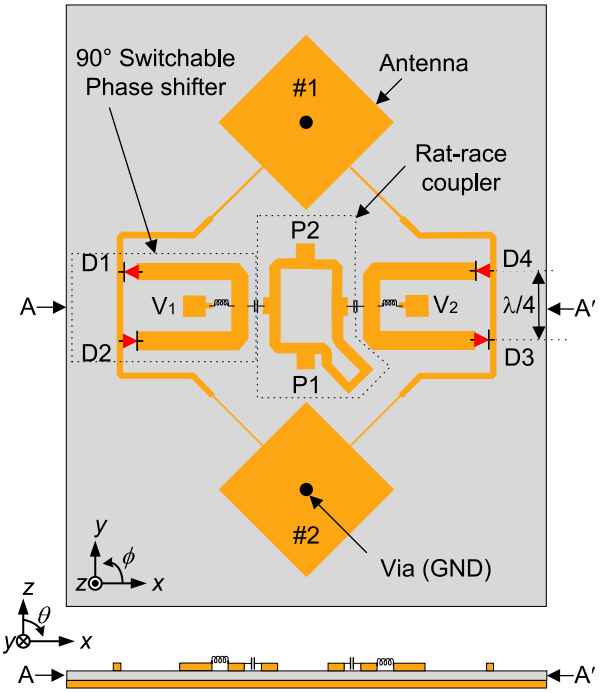

FIGURE 2. Geometrical configuration and cross-sectional view of the proposed antenna.

the center of the patches act as a common DC grounding for both switches.

B. OPERATING MECHANISM

Table 1 shows the operational modes of the proposed antenna. The SPDT switches can generate four switching combinations for ports P1 and P2. Overall, the proposed antenna offers eight operating modes I∼VIII. The proposed antenna can generate four polarization states; right-handed circular polarization (RHCP), left-handed circular polarization (LHCP), horizontal linear polarization (HLP), and vertical linear polarization (VLP). It can be seen that by changing only the ports, the polarization states can be switched. Considering that the current distribution of each polarization state is not the same, different radiation patterns can be generated. In that way, dual beams can be generated for each quad-polarization state.

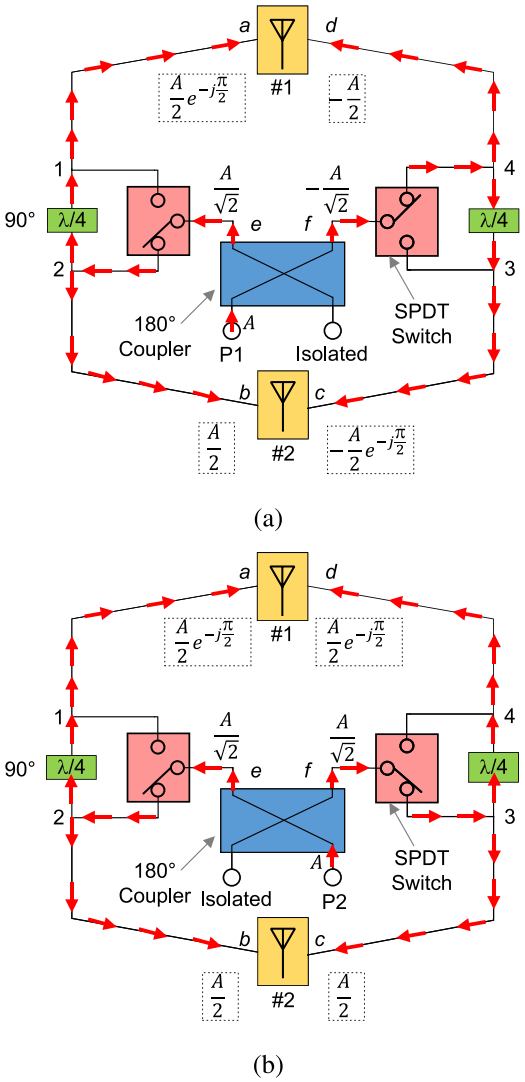

FIGURE 3. Operating mechanism of the proposed antenna. (a) Mode I. (b) Mode VII.

Fig. 3 shows the operating mechanism of the proposed antenna. In the case of mode I, when the signal with amplitude A is fed from port P1 of the 180° coupler, the signal splits equally with 180° out-of-phase into its two output ports, e, f as shown in Fig. 3(a).

$$e = \frac{A}{\sqrt{2}}, f = -\frac{A}{\sqrt{2}}. \tag{1}$$

The signal travels following the branch with the diode ON condition of the SPDT switches. The other branch of the SPDT switches acts as an open circuit due to the $\lambda/2$ length. The impedance looking towards the OFF diode becomes infinite and no signal travels to that path. In the case of mode I, the signal again splits at points 2 and 4. Due to the $\lambda/4$ delay line, an extra 90° phase difference occurs between the patch elements #1 and #2. Thus the orthogonal signals of the two patch elements are distributed like below,

$$a = \frac{A}{2}e^{-j\frac{\pi}{2}}, b = \frac{A}{2},$$
$$c = -\frac{A}{2}e^{-j\frac{\pi}{2}}, d = -\frac{A}{2}. \tag{2}$$

As seen from the above equation, the orthogonal signals of the patches have the same amplitude but with a 90° phase difference. Thus, RHCP will be generated. Besides, the sum radiation pattern is generated as the two patches are in phase. On the other hand, LHCP is achieved for the operating mode V when the signal is fed from port P2. In this case, as shown in the Appendix, a difference radiation pattern is generated as the signals a, c and b, d are in in-phase as opposed to the sum condition.

Fig. 3(b) shows the operating mechanism for the operating mode VII. When the signal is fed from port P2, the signal splits to the output ports like below,

$$e = \frac{A}{\sqrt{2}}, f = \frac{A}{\sqrt{2}}. \tag{3}$$

Due to the operating mode VII condition, the signal distributes to the patches as shown below.

$$a = d = \frac{A}{2}e^{-j\frac{\pi}{2}},$$
$$b = c = \frac{A}{2}. \tag{4}$$

This condition also creates a 90° phase difference between the patch elements #1 and #2 instead of between the orthogonal signals like the mode I. Thus, VLP is generated with tilted beam patterns following the below equation.

$$\theta_m = \pm \sin^{-1}\left(\frac{\lambda_0}{4d}\right) \tag{5}$$

where θ_m, λ_0, and d are the beam angle, free-space wavelength, and patch spacing between the antenna elements #1 and #2, respectively. For port P1, HLP is generated with the signal distributions shown in the Appendix.

This design layout offers three benefits. Firstly, due to the dual port setup, both polarizations can be directed in the same way without altering the switch states. This enhances agility in applications involving Multiple-Input Multiple-Output (MIMO) and diversity. Secondly, the design is achieved in a single-layer structure with a low complexity level. Despite having 4 switches, only 2 biasing lines are needed, significantly simplifying the biasing network.

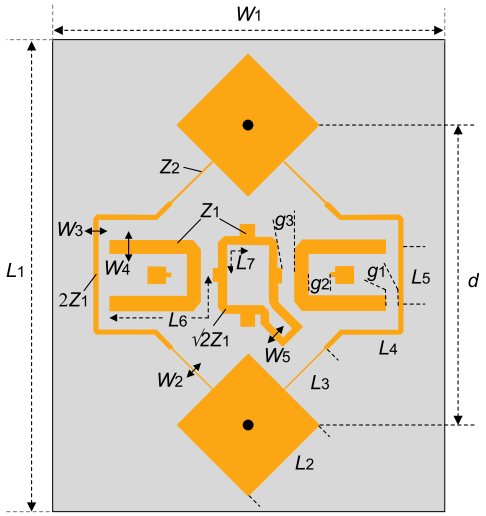

FIGURE 4. Optimized layout of the proposed antenna.

TABLE 2. Final optimum parameter values of Fig. 4.

Param.	Value	Param.	Value	Param.	Value
L_1	95.00 mm	L_2	17.00 mm	L_3	9.72 mm
L_4	18.59 mm	L_5	9.10 mm	L_6	19.69 mm
L_7	9.72 mm	W_1	70.00 mm	W_2	0.17 mm
W_3	0.70 mm	W_4	2.40 mm	W_5	1.40 mm
g_1	0.20 mm	g_2	0.20 mm	g_3	0.20 mm
Z_1	50 Ω	Z_2	162 Ω	d	50.00 mm

C. DESIGN

Fig. 4 shows the optimized circuit dimensions of the proposed antenna. The antenna is designed for 5.8 GHz by the Momentum of Keysight Technologies' Advanced Design System. Here, L, W, g, and Z represent the length, width, gap, and characteristic impedance of the lines, respectively. Table 2 shows the optimum parameter values. The total dimension of the antenna is W_1 (= 70 mm) × L_1 (= 95 mm). The antenna elements with dimensions of $L_2 = 17$ mm are used and separated by $d = 0.97\lambda_0$ (= 50.00 mm). The two antenna elements are connected by a 100-Ω ($2Z_1$) microstrip line ($W_3 = 0.7$ mm, $L_4 = 18.59$ mm, and $L_5 = 9.1$ mm). An impedance transformer of 162 Ω (Z_2) is used with the dimensions of $W_2 = 0.17$ mm, $L_3 = 9.72$ mm. The SPDT switches are designed with $Z_1 = 50\,\Omega$ and $W_4 = 2.4$ mm. The other parameters are $L_6 = 19.69$ mm and $L_7 = 9.72$ mm. All the gaps (g_1, g_2, and g_3) are kept at 0.2 mm. The antenna is employed 0.8-mm thick polytetrafluoroethylene (PTFE) substrates with a permittivity of 2.15 and dielectric loss tangent of 0.001 to demonstrate the idea experimentally. In the simulation, the PIN diodes' ON and OFF conditions are realized by using the short and open circuits, respectively.

Fig. 5 shows the simulated surface current distributions of the proposed antenna for modes I and V. Current distributions for difference phase instants from 0° to 270° with an interval of 90° are shown to find out the polarization state for each port. When the signal is fed from port P1 as shown in

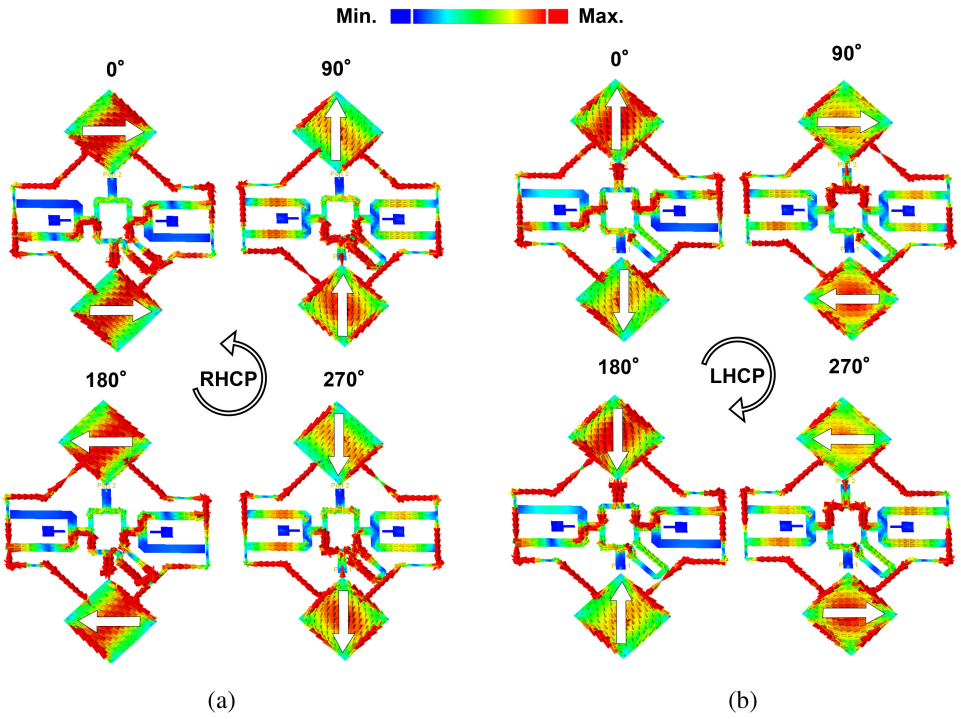

FIGURE 5. Simulated current distributions of the proposed antenna for the diodes D2 and D4 ON conditions with different phase instants from 0° to 270° with an interval of 90°. (a) Mode I (Port P1): counter-clockwise rotation is observed. (b) Mode V (Port P2): clockwise rotation is observed.

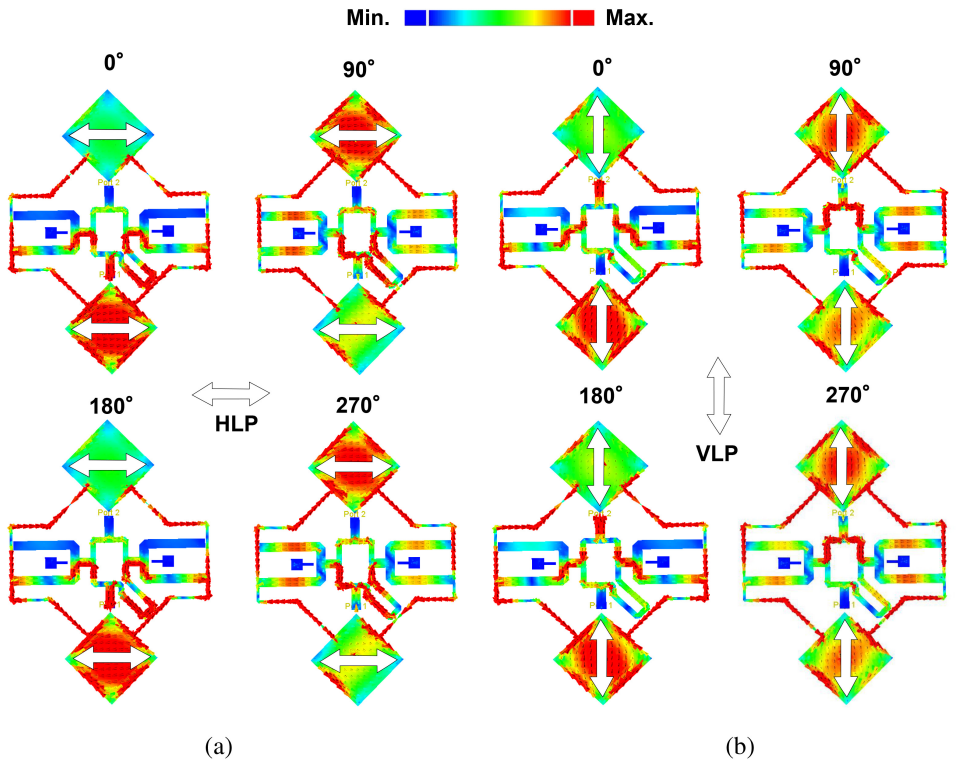

FIGURE 6. Simulated current distributions of the proposed antenna for the diodes D2 and D3 ON conditions with different phase instants from 0° to 270° with an interval of 90°. (a) Mode III (Port P1): HLP is observed. (b) Mode VII (Port P2): VLP is observed.

Fig. 5(a), a counter-clockwise field rotation with increasing phase is observed. Consequently, this polarization sense is RHCP. In contrast, it is clear from Fig. 5(b) that LHCP is generated for port P2. In both cases, the surface current is drawn at the frequency where the lowest axial ratio (AR) is observed. In the case of port P1, the two antenna elements

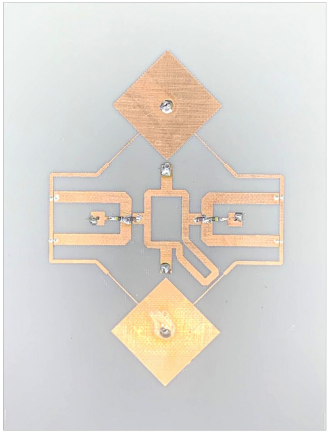

FIGURE 7. 5.8 GHz-band prototype of the proposed antenna (70 mm × 95 mm).

have the same phase and therefore, generate a sum radiation pattern. On the other hand, a difference radiation pattern is generated for port P2 as the two antenna elements are 180° out-of-phase.

Fig. 6 shows the simulated current distributions of the proposed antenna at 5.8 GHz for modes III and VII. HLP and VLP are radiated for ports P1 and P2, respectively. In both conditions, one antenna element is 90° ahead of the other antenna element. As a result, both polarization states show a tilted beam radiation pattern.

III. MEASUREMENT RESULTS

To validate the simulated results, a 5.8 GHz-band prototype antenna has been fabricated and measured. Fig. 7 illustrates the photograph of the fabricated proposed antenna. The dimension of the ground plane of the antenna is 70 mm × 95 mm. Four PIN diodes of Skywork's DSG9500-000 are used in the proposed antenna. For PIN diode switching, positive (+1.0 V) and negative (−1.0 V) switching voltages are applied.

Fig. 8 shows the measured S-parameters for the diode ON conditions and compares them with simulated results. The measured reflection coefficients ($|S_{11}|$ and $|S_{22}|$) are much wider than the simulated results. The measured results have achieved a good agreement with the simulated results in the frequency range from 5.6 GHz to 5.9 GHz for all four conditions. The simulated and measured 10-dB return loss bandwidths considering their respective center frequency for both ports are around 4% and 9%, respectively. High port isolations ($|S_{21}|$) of ∼19 dB are achieved at 5.77 GHz. A mismatch is observed between the measured and simulated performances of the antenna. The main reason for this inconsistency is attributed to the utilization of the ideal ON (short circuit) and OFF (open circuit) conditions of the diode during simulation. This occurs because the parasitic components, which are not taken into account during simulation, have an impact on the measured performances.

Fig. 9 shows the measured and simulated CP and LP switching with simulated results. For diodes D2 and D4 ON conditions shown in Fig. 9(a), both ports achieve AR

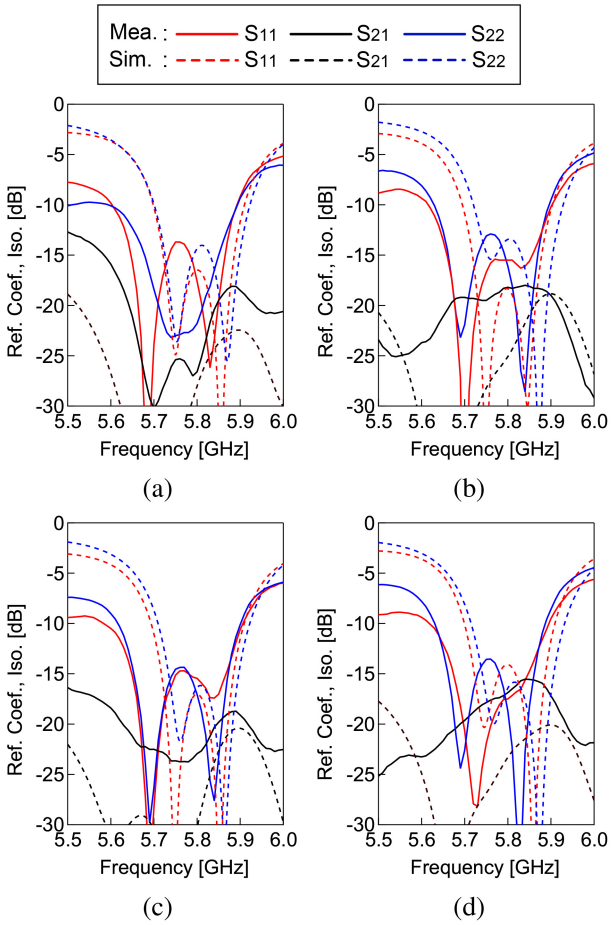

FIGURE 8. Measured and simulated reflection coefficient and isolation of the fabricated antenna for the diodes (a) D2, D4: ON, (b) D1, D3: ON, (c) D2, D3: ON, and (d) D1, D4: ON conditions.

≤ 3 dB with a slight frequency shifting from simulation. A measured 3-dB AR bandwidth of 0.7% is obtained for Port 2 with a minimum value of 1.02 dB at 5.73 GHz. The overlapped bandwidth for $|S_{11}| < -10$ dB and AR<3 dB is about 6%. In the case of port P1, the minimum AR is observed at 5.77 GHz. Similar CP characteristics can be observed for Fig. 9(b) as well. It is apparent from Figs. 9(a) and (b) that good CP performance can be guaranteed over the −10-dB impedance bandwidth. The antenna can be used in some narrow-band applications, for example, fixed (point-to-point) communications as the AR bandwidth of the proposed antenna is narrow [17]. The wideband feeding technique can be employed to broaden the AR bandwidth [12], [13]. Figs. 9(c) and (d) show LP characteristics of the proposed antenna. In both cases, ports P1 and P2 account for HLP and VLP, respectively. Thus, the quad-polarization switching concept is found to be feasible.

Fig. 10 shows the measured and simulated far-field radiation patterns at $\phi = 90°$-plane. The simulation considers infinite ground plane size. All the graphs are drawn at their lowest AR frequency. It is worthwhile to point out here that modes I and V can be used as a monopulse antenna, where port P1 produces a sum beam, and port P2 produces

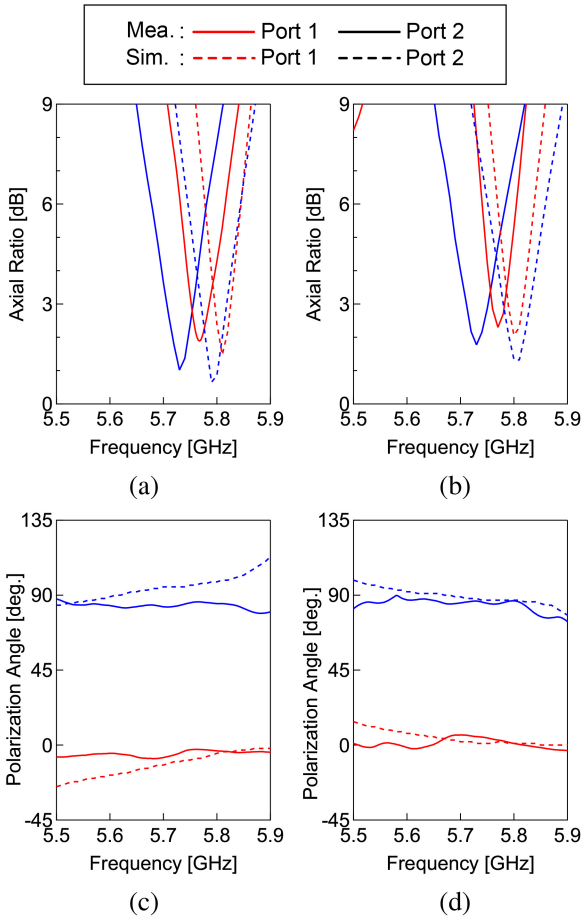

FIGURE 9. Measured and simulated polarization state of the fabricated antenna in the $\phi = 90°$-plane for the diodes (a) D2, D4: ON (Ports P1 and P2 are measured at $\theta = 0°$ and $-26°$, respectively). (b) D1, D3: ON (Ports P1 and P2 are measured at $\theta = 0°$ and $-26°$, respectively). (c) D2, D3: ON, and (d) D1, D4: ON conditions.

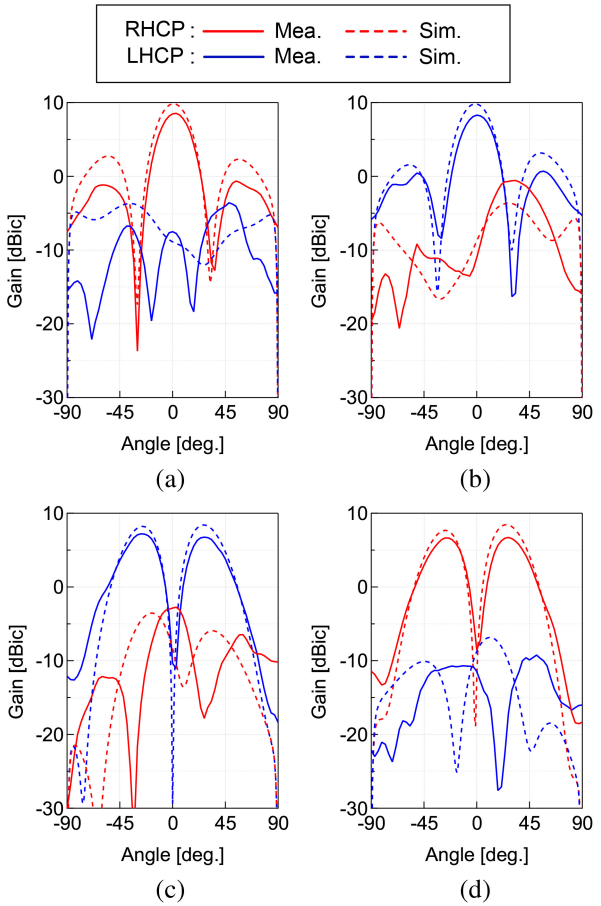

FIGURE 10. Measured and simulated radiation patterns in the $\phi = 90°$-plane. (a) Mode I. (b) Mode II. (c) Mode V. (d) Mode VI.

a difference beam. Similarly, modes II and VI can be also used as a monopulse antenna with similar radiation patterns for both ports but the CP polarization sense is altered. The realized gain is above 8.5 dBic in the measurement compared to the 10-dBic gain in the simulation for both modes. It can be seen from Fig. 10 that CP switching from RHCP to LHCP can be achieved by changing its port or by diode condition. Better than 7-dBic realized gain is measured in both modes. In all cases, the co-polarization components are at least 15 dB better than its cross-polarization components.

Fig. 11 displays the radiation patterns of the linear polarized states for the operating modes III, IV, VII, and VIII. Both the measured and simulated data are shown for comparison. The antenna's performance was evaluated at a frequency of 5.8 GHz in both simulation and measurement. The measured gains of the array antenna are better than 7.5 dBi for port P1 observed at $+15°$ and $-15°$ in the $\phi = 90°$-plane for the operating modes III and IV, respectively. In the case of operating modes VII and VIII shown in Figs. 11(c) and (d), the measured peak angle was observed at $\mp 12°$, respectively. The measured realized gain was better than 7 dBi in both operating modes. In all cases, the measured cross-polarization suppressions were approximately >20 dB. Figs. 11(a), (b) and (c), (d) demonstrate that the proposed antenna exhibits distinct bi-directional radiation patterns for ports P1 and P2. Simulated gains are around 2 dB higher than the measurement. Besides, the measured peak angle has a slight deviation from the simulated results. The proposed antenna has the limitation of adjusting the patch-to-patch distance ($d = 0.97\lambda_0$) due to the placement of the feeding network on the same layer with the antennas. As a result, grating lobes appear. By using the high permittivity substrate, this limitation of this antenna can be solved. The microwave circuits can be miniaturized in high permittivity substrate because the length of the transmission line depends on the effective wavelength, which is less than the free-space wavelength. On the other hand, antenna separation depends on the free-space wavelength, which is not affected by the substrate permittivity. But, in this case, radiation performance might be worse.

Fig. 12 shows the simulated radiation efficiency and gain for ideal and diode equivalent model for Mode I. It is not possible to include the equivalent circuit of the parasitic element (diode) in the ADS Momentum. To understand the effect of the PIN diode, the antenna is also checked by using the FEM of EMPro. Here, the solid and dashed lines present the diode equivalent circuit and ideal model, respectively. For

TABLE 3. Comparison of the proposed antenna with previously reported antennas.

Ref.	Freq. [GHz]	Size [mm^2]	No. of Pol.	Beam/Pol.	No. of Ports	No. of Diodes	No. of Subs.	BW [%] (LP/CP)	AR OL BW [%]	Gain (dBi/dBic)
[4]	2.40	NA†	2 LP	1	1	NA†	NA†	22.9	NA†	4.2
[6]	5.40	74 × 74	2 CP	5	1	40	3	17	55	10.1
[7]	3.80	65 × 120	2 LP	3	2	8	4	29	NA†	8.2
[8]	5.00	39 × 39	2 LP, CP	2	1	16	3	16	26	3.09/4.38
[9]	5.20	60 × 60	3 LP, 2 CP	1	1	17	3	9.74/38.7	28	8.73/8.2
[10]	2.40	200 × 200	3 LP	5	1	16	3	8.3	NA†	3.5
[11]	2.40	200 × 200	4 LP	1	1	16	2	13	NA†	12.6
[12]	1.85	245 × 243	2 LP, 2 CP	1	2	6	2	28.4/60.3	26.3	4.2/2.8
[13]	2.40	106 × 80	2 LP, 2 CP	1	1	8	3	84.5/120	100	7.8/7.8
[17]	2.55	120 × 120	2 CP	1	1	16	2	15.2	23	9.6
[20]	2.45	74 × 74	2 CP	4	1	12	3	13.1	25	11.23
[21]	2.40	100 × 100	LP	12	4	NA†	1	1.25	NA†	8.2
Proposed	**5.80**	**70 × 90**	**2 LP, 2 CP**	**2**	**2**	**4**	**1**	**9.0**	**6**	**7.6/8.5**

† NA: Not applicable or not found in the literature. AR OL BW: Axial ratio overlapped bandwidth

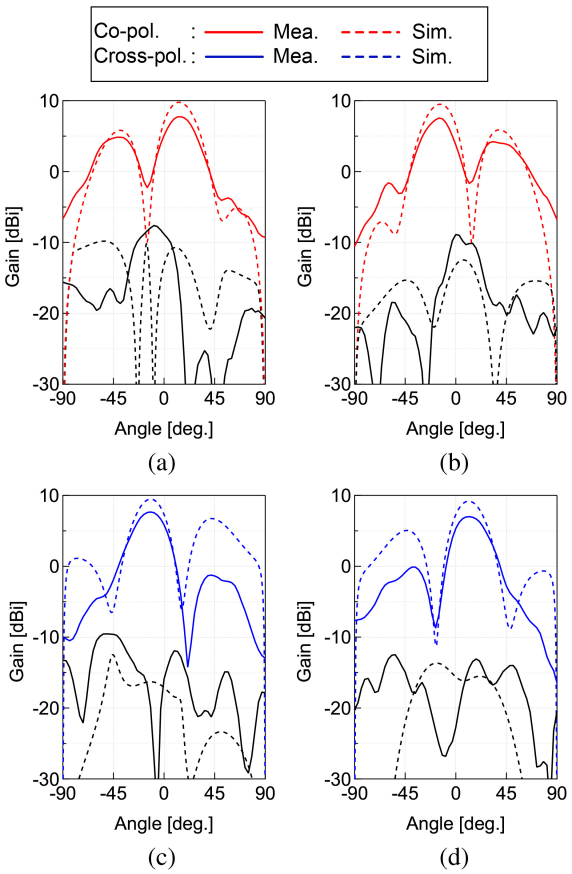

FIGURE 11. Measured and simulated radiation patterns in the $\phi = 90°$-plane. (a) Mode III. (b) Mode IV. (c) Mode VII. (d) Mode VIII.

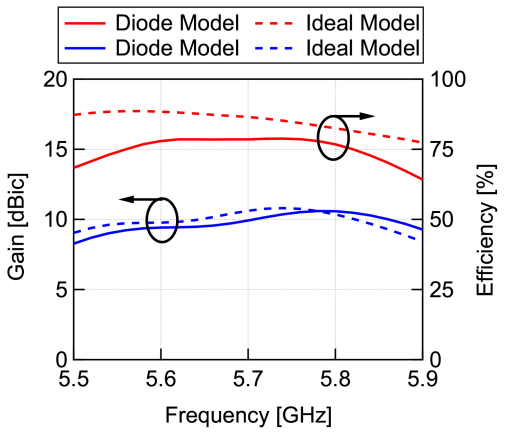

FIGURE 12. Simulated radiation efficiency and gain for ideal and diode equivalent model for Mode I using EMPro software.

an equivalent circuit to realize the ON and OFF states of the diode, a 3-Ω resistor and a 0.025-pF capacitor are used. The ideal model's ON and OFF states are realized by open and short circuits, respectively. In EMPro, the center frequency is around 150 MHz lower than the ADS for the same layout of the proposed antenna. Around 0.45 dB loss is observed due to the PIN diode at 5.64 GHz. The simulated antenna's efficiency of the antenna is around 75% considering the equivalent circuit model of the PIN diode. The measured efficiency can be quite low due to the lower gain than the simulation.

Fig. 13 shows the measured radiation patterns versus angle and frequency for the operating modes I, III, V, and VII in the $\phi = 90°$-plane. In the case of mode I, the measured radiation performance for port P1 is depicted in Fig. 13(a), which shows the radiation peak occurs at $\theta = 0°$ (sum pattern) over the shown frequency band. In contrast, difference pattern is observed for port P2 in Fig. 13(b). As the switched-line phase shifter has a narrow frequency band, the difference pattern performance varies with frequency. Similarly, tilted beam angle shifts for modes IV and VIII as shown in Figs. 13(c) and (d), respectively. It can be seen from the figure that the beam tilted towards $-\theta$ for port P1 and $+\theta$ for port P2, respectively.

Table 3 shows the comparison of the proposed antenna with previously reported antennas. The comparison is shown in terms of the size, the number of polarization, beams per polarization, performance, and the number of ports, diodes,

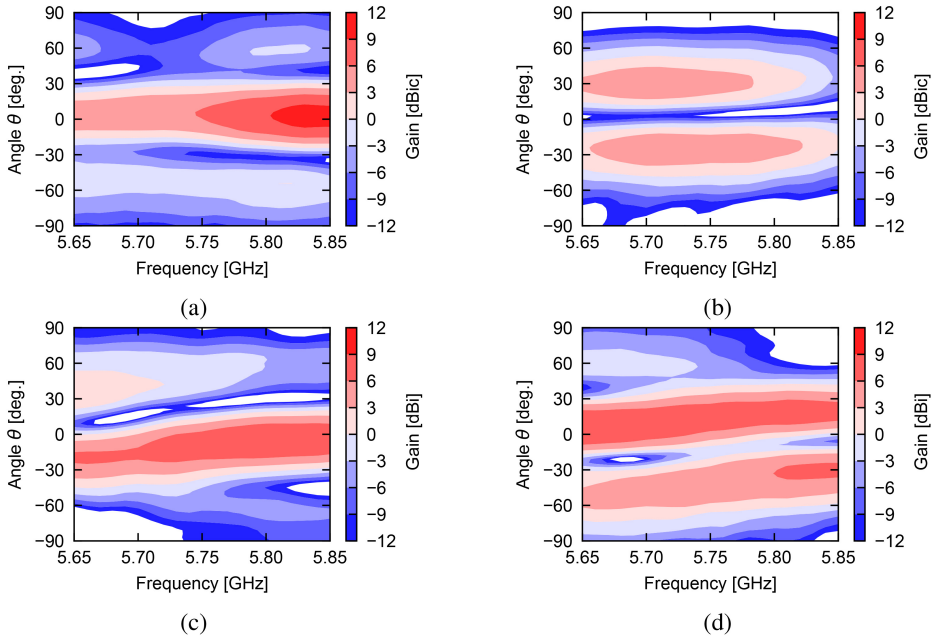

FIGURE 13. Measured radiation patterns as a function of frequency in the $\phi = 90°$-plane. (a) Mode I. (b) Mode V. (c) Mode IV. (d) Mode VIII.

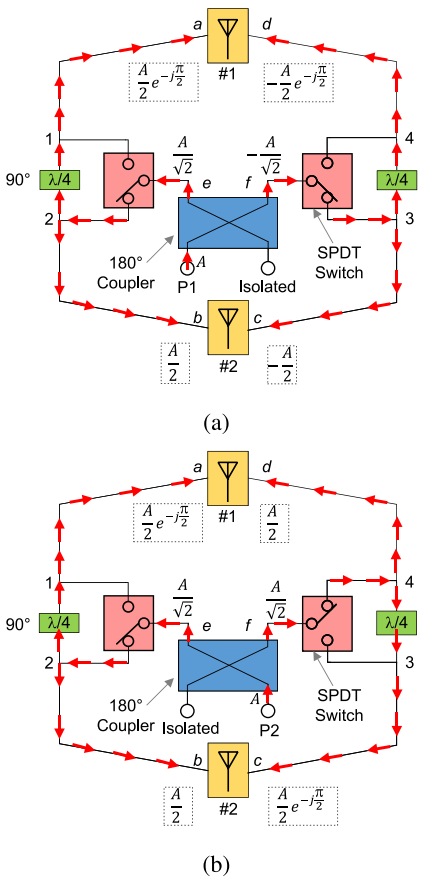

FIGURE 14. Operating mechanism of the proposed antenna. (a) Mode III. (b) Mode V.

and substrate to validate the advantage of the proposed antenna. It is evident from the comparison that the proposed antenna has many novelties with a good balance of overall size and functionality. Similar functional antennas require multi-substrate and lots of RF switches. The performance of the antenna is comparable to other reported antennas. In short, this study is one of the few antennas to provide polarization and beam agility simultaneously with a compact size and a low profile.

IV. CONCLUSION

In this study, a simultaneous polarization and beam switchable array antenna is developed. The rat-race coupler and switched-line phase shifters create the necessary phase difference between the antenna elements or the orthogonal feed networks. By changing the input ports of the rat-race coupler, polarization and radiation patterns can be switched. The two ports have high isolation. As a result, the proposed antenna can be used in MIMO applications. The measured results of the fabricated prototype antenna agree well with the simulated results with the capability of simultaneous polarization and beam switching functionality, wide bandwidth, and ease of design and fabrication.

APPENDIX

Fig. 14 shows the operating mechanism of the proposed antenna. (a) Mode III. (b) Mode V.

ACKNOWLEDGMENT

The authors are grateful to Dr. Takayuki Tanaka, Saga University for his suggestions and fruitful discussions.

REFERENCES

[1] S. Gao, A. Sambell, and S. S. Zhong, "Polarization-agile antennas," *IEEE Antennas Propag. Mag.*, vol. 48, no. 3, pp. 28–37, Jun. 2006.

[2] J. F. Valenzuela-Valdes, M. A. Garcia-Fernandez, A. M. Martinez-Gonzalez, and D. Sanchez-Hernandez, "The role of polarization diversity for MIMO systems under Rayleigh-fading environments," *IEEE Antennas Wireless Propag. Lett.*, vol. 5, pp. 534–536, 2006.

[3] J. Hu, Z.-C. Hao, and Y. Wang, "A wideband array antenna with 1-bit digital-controllable radiation beams," *IEEE Access*, vol. 6, pp. 10858–10866, 2018.
[4] J. Ren et al., "Radiation pattern and polarization reconfigurable antenna using a dielectric liquid," *IEEE Trans. Antennas Propag.*, vol. 68, no. 12, pp. 8174–8179, Dec. 2020.
[5] *Base Station (BS) Radio Transmission and Reception (Release 17), V17.5.0*, 3GPP Standard TS 38.104, Apr. 2022.
[6] C. Liu, Y. Li, T. Liu, Y. Han, J. Wang, and S. Qu, "Polarization reconfigurable and beam-switchable array antenna using switchable feed network," *IEEE Access*, vol. 10, pp. 29032–29039, 2022.
[7] G. A. Ramírez et al., "Reconfigurable dual-polarized beam-steering broadband antenna using a crossed-strips geometry," *IEEE Antennas Wireless Propag. Lett.*, vol. 20, pp. 1379–1383, 2021.
[8] W. Li, Y. M. Wang, Y. Hei, B. Li, and X. Shi, "A compact low-profile reconfigurable metasurface antenna with polarization and pattern diversities," *IEEE Antennas Wireless Propag. Lett.*, vol. 20, pp. 1170–1174, 2021.
[9] P. Liu, W. Jiang, S. Sun, Y. Xi, and S. Gong, "Broadband and low-profile penta-polarization reconfigurable metamaterial antenna," *IEEE Access*, vol. 8, pp. 21823–21831, 2020.
[10] C. Gu et al., "Compact smart antenna with electronic beam-switching and reconfigurable polarizations," *IEEE Trans. Antennas Propag.*, vol. 63, no. 12, pp. 5325–5333, Dec. 2015.
[11] J.-S. Row and Y.-J. Huang, "Reconfigurable antenna with switchable broadside and conical beams and switchable linear polarized patterns," *IEEE Trans. Antennas Propag.*, vol. 66, no. 7, pp. 3752–3756, Jul. 2018.
[12] M. Liu, Z. J. Zhai, F. Lin, and H. J. Sun, "Wideband quad-polarization-reconfigurable bidirectional antenna with a simple wideband switchable feeding network," *IEEE Antennas Wireless Propag. Lett.*, vol. 22, pp. 1346–1350, 2023.
[13] X. Ding, Z. Zhao, Y. Yang, Z. Nie, and Q. H. Liu, "Wideband quad-polarization reconfigurable antenna using switchable feed network with stable unidirectional radiation patterns," *IEEE Access*, vol. 6, pp. 73434–73443, 2018.
[14] L. Kang, H. Li, B. Tang, X. Wang, and J. Zhou, "Quad-polarization-reconfigurable antenna with a compact and switchable feed," *IEEE Antennas Wireless Propag. Lett.*, vol. 20, pp. 548–552, 2021.
[15] M. Hasan, E. Nishiyama, and I. Toyoda, "The multi-layer approach of polarization agile oscillating-type active integrated array antennas for RF transmitter front-end," *Int. J. Microw. Wireless Technol.*, vol. 15, no, 4, pp. 600–608, May 2023.
[16] Y.-M. Lin, J.-S. Yang, and J.-S. Row, "A design for suspended patch antenna with switchable polarization," *Microw. Opt. Technol. Lett.*, vol. 58, no. 6, pp. 1333–1337, Jun. 2016.
[17] W. Li et al., "Polarization-reconfigurable circularly polarized planar antenna using switchable polarizer," *IEEE Trans. Antennas Propag.*, vol. 65, no. 9, pp. 4470–4477, Sep. 2017.
[18] I. T. McMichael, "A mechanically reconfigurable patch antenna with polarization diversity," *IEEE Antennas Wireless Propag. Lett.*, vol. 17, pp. 1186–1189, 2018.
[19] H. Su, I. Shoaib, X. Chen, and T. Kreouzis, "Optically tuned polarisation reconfigurable antenna," in *Proc. IEEE Asia–Pacific Conf. Antennas Propag. (APCAP2012)*, Singapore, 2012, pp. 265–266.
[20] H. Sun, X. Ge, W. He, and L. Zhao, "A reconfigurable antenna with sum and difference patterns for WLAN access points," *IEEE Antennas Wireless Propag. Lett.*, vol. 19, pp. 1073–1077, 2020.
[21] A. Pal, A. Mehta, D. Mirshekar-Syahkal, and H. Nakano, "A twelve-beam steering low-profile patch antenna with shorting vias for vehicular applications," *IEEE Trans. Antennas Propag.*, vol. 65, no. 8, pp. 3905–3912, Aug. 2017.
[22] M. Hasan, E. Nishiyama, and I. Toyoda, "A multi-beam array antenna employing simple 4×2 beam-forming network integrating magic-T and hybrid coupler," in *Proc. Int. Symp. Antennas Propag. (ISAP2022)*, Sydney, NSW, Australia, 2022, pp. 437–438.
[23] M. Hasan, E. Nishiyama, T. Tanaka, and I. Toyoda, "A dual-beam switchable self-oscillating Ku-Band active array antenna integrating positive feedback type Push-Push oscillator and PSK modulator," *Prog. Electromagn. Res. C*, vol. 116, pp. 181–192, Nov. 2021.
[24] A. A. Omar et al., "A planar, polarization-switchable endfire and ±broadside millimeter-wave antenna array without lumped components," *IEEE Trans. Antennas Propag.*, vol. 70, no. 5, pp. 3864–3869, May 2022.
[25] M. Hasan, E. Nishiyama, T. Tanaka, and I. Toyoda, "Three-state pattern reconfigurable active antenna integrated with Gunn oscillator and switched-line phase shifter," *Electron. Lett.*, vol. 59, no. 12, Jun. 2023, Art. no. e12839.

MAODUDUL HASAN (Member, IEEE) was born in Chattogram, Bangladesh, in 1992. He received the B.Sc. degree in electronics and communication engineering from the Khulna University of Engineering and Technology, Khulna, Bangladesh, in 2014, and the M.E. and Dr.Eng. degrees in communication engineering from Saga University, Saga, Japan, in 2019 and 2022, respectively.

From 2014 to 2017, he worked as a Transmission Engineer with Huawei Technologies Bangladesh Ltd. Since April 2022, he has been a Project Assistant Professor with Saga University. His research interests include active integrated antennas and reconfigurable antenna designs.

Dr. Hasan was a recipient of the Honourable President Award from Saga University; the Student Presentation Award at ICETC2020; the SRW Research Committee Award in 2019; the IEEE AP-S Japan Student Award in 2022 and IEEE AP-S Student Encouragement Award in 2019, Tokyo Chapter; the Best Paper Awards at ECCE2023, ICPRSET2022, and APCAP2019; and the 2018 Excellent Student Award of the IEEE Fukuoka Section. He is a member of IEICE.

EISUKE NISHIYAMA (Member, IEEE) received the Doctor of Engineering degree from Kyushu University in 2005. He is currently working as an Associate Professor with the Faculty of Science and Engineering, Saga University, Japan. From 2007 to 2008, he was a Visiting Scholar of Electrical Engineering with the University of California at Los Angeles. His research interests are in reconfigurable microstrip antennas and rectennas. He served as the Vice-Chair of the IEEE Antennas and Propagation Society Fukuoka Chapter from 2011 to 2012 and the Chair from 2013 to 2014, respectively.

ICHIHIKO TOYODA (Member, IEEE) received the B.E., M.E., and Dr.Eng. degrees in communication engineering from Osaka University, Osaka, Japan, in 1985, 1987, and 1990, respectively.

From 1990 to 2011, he was engaged in research and development of the 3-D and uniplanar MMICs, ultra-high-speed digital ICs, millimeter-wave high-speed wireless access systems, and their applications with NTT Laboratories and NTT Electronics Corporation. He was also active in developing IEEE 802.11, 802.15, and other national standards. He is currently a Professor and the Dean of the Faculty of Science and Engineering, Saga University, Japan. He published six book chapters. His current interests concern microwave circuits, antennas, and their integration technologies, including wireless power transfer. He received the 1993 Young Researcher's Award presented by IEICE, Japan; the Japan Microwave Prize presented at APMC1994; the 18th Telecom System Technology Award from the Telecommunications Advancement Foundation; the 2004 Electronics Society Award from IEICE, Japan; the First Prize for Propagation and Antenna Measurements at EuCAP2010; the 2010 and 2016 Best Paper Awards from IEICE, Japan; the 2020 Best Paper Award from IEEJ, and many conferences and NTT R&D awards. He was also recognized as an Excellent Educator by Saga University in 2017. He was a Guest Editor of a 1998 special issue on "3D-Components and Active Circuits" of the *International Journal of RF and Microwave Computer-Aided Engineering* and a Guest Editor-in-Chief of a 2016 special issue on "Microwave Researches in Universities" of the Institute of Electronics, Information and Communication Engineers (IEICE) Transactions on Electronics. He was a Councilor, Tokyo Section and Kyushu Section, IEICE, a GA Member of the European Microwave Association (EuMA), and the Chair of IEEE AP-S Fukuoka Chapter. He also served Technical Committee on Electron Devices of the Institute of Electrical Engineers of Japan (IEEJ) as a Secretary, the Vice-Chair, and the Chair. He also served on many other technical committees of IEICE and IEEJ, Japan. He is a Senior Member of IEICE and IEEJ, and a member of EuMA.